Quantitative Analyses of the Interfacial Properties of Current Collectors at the Mesoscopic Level in Lithium Ion Batteries by Using Hierarchical Graphene

Mingzhan Wang,[∇] Hao Yang,[∇] Kexin Wang,[∇] Shulin Chen, Haina Ci, Liurong Shi, Jingyuan Shan, Shipu Xu, Qinci Wu, Chongzhen Wang, Miao Tang, Peng Gao, Zhongfan Liu,* and Hailin Peng*

ACCESS | Metrics & More | Article Recommendations | Supporting Information

ABSTRACT: At the mesoscopic level of commercial lithium ion battery (LIB), it is widely believed that the poor contacts between current collector (CC) and electrode materials (EM) lead to weak adhesions and large interfacial electric resistances. However, systematic quantitative analyses of the influence of the interfacial properties of CC are still scarce. Here, we built a model interface between CC and electrode materials by directly growing hierarchical graphene films on commercial Al foil CC, and we performed systematic quantitative studies of the interfacial properties therein. Our results show that the interfacial electric resistance dominates, i.e. ~2 orders of magnitude higher than that of electrode materials. The interfacial resistance could be eliminated by hierarchical graphene interlayer. Cathode on CC with eliminated interfacial resistance could deliver much improved power density outputs. Our work quantifies the mesoscopic factors influencing the battery performance and offers practical guidelines of boosting the performance of LIBs and beyond.
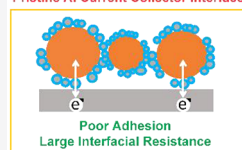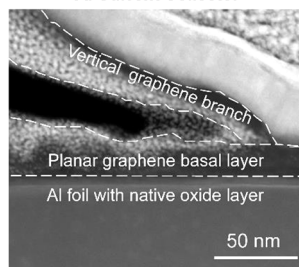
The lithium ion battery (LIB) has revolutionized the consumer electronics and electric vehicles industries, and it is finding its way to prospective smart power grids.[1,2] Strenuous efforts, which include the consummation of electrode materials,[3−6] and the electrolyte recipes[7,8] at the single component level and the improvement of the manufacturing process,[9,10] have been devoted toward safer and higher energy/power density of LIBs. However, during this uphill progress, the basic configuration of LIB remains conservative, namely, it consists of cathode, anode, electrolyte, separator, and current collector, etc.[1] Therein, a current collector (CC), which mechanically supports the electrode materials (EM) and electronically bridges the internal electrochemical and external electric circuit, is an indispensable player in LIB.[11] Material candidates of current collector should meet the following criteria simultaneously: have good electric conductivity; have robust chemical and electrochemical stability, be inexpensive and easily available; and be lightweight. In compliance with such demanding criteria, commercial CCs for the cathode and anode electrode are almost confined to Al foil and Cu foil, respectively.

However, there are intrinsic defects originating from the mesoscopic electrode configuration. On one hand, for the sake of decent energy density and minimized side reactions, the active materials are usually on the order of micrometers;[6,12,13]

on the other hand, as schematically shown in Figure 1a, micrometer-sized active materials have limited interface contacts with bare Al foil (denoted hereafter as "b-Al"). The electrode configuration thus falls into a dilemma.

Consequently, EM are prone to delaminating from bare current collector due to poor adhesion and a large interfacial resistance exists at the CC/EM interface, because of limited electric channels. Because of the presence of a native electrically insulating aluminum oxide layer on Al foil, this problem is particularly highlighted on the cathode/Al foil interface.[14,15] The awesome interfacial resistance impairs the power properties (such as fast charging and high-power-discharging) of LIBs dramatically.[16] Thus, for the amelioration of LIB, it is of primary significance to revisit the mesoscopic electrode configuration with a focus on the interfacial properties of current collector. Roughened Al current collector,[17,18] carbon-coated Al foil[19,20] (or its derivatives of
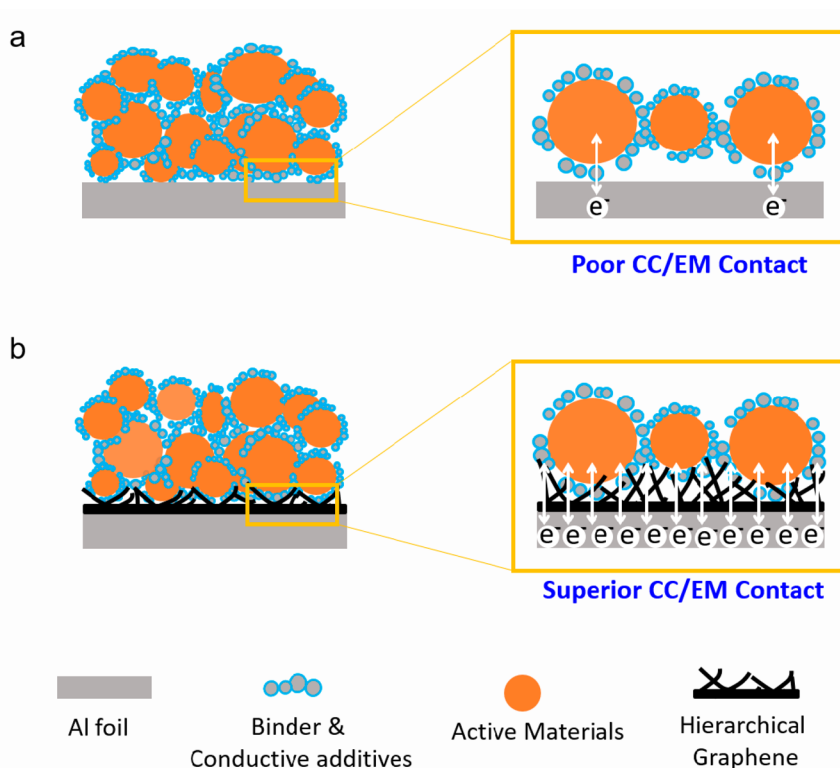
Figure 1. Schematic illustrations showing the model interface between (a) bare Al foil current collector (CC) and (b) hierarchical-graphene-engineered Al foil CC with electrode materials (EM), respectively.

carbon nanotube-coated Al foil[21] or graphene-coated Al foil[22,23]), and vertical graphene current collectors,[24] etc., have been proposed to enhance the CC/EM interface. Despite these progress achieved, few works are dedicated to the quantitative analysis as to the interfacial properties at the mesoscopic level.

Here, we approach this issue by building a model interface of Al foil current collector, i.e., with directly synthesized hierarchical graphene (denoted hereafter as "hG-Al"), as schematically shown in Figure 1b. Systematic quantitative studies, including mechanical, electric, and electrochemical tests, are performed to reveal how the hierarchical graphene interlayer influences the performance of electrodes quantitatively at the mesoscopic level. Mechanical tests indicate that the adhesion strength of electrode on hG-Al current collector was improved by ca. 5-fold, compared to that on pristine bare Al foil. Electric tests show that the interfacial resistance is ca. 2 orders of magnitude higher than electrode materials resistance, being dominant in the entire electrode. By contrast, the hierarchical graphene interlayer could almost eliminate that awesome interfacial resistance. Ultimately, the electrochemical performances, particularly the power performances of electrodes with a hierarchical graphene interlayer, are significantly improved.

The growth of graphene on Al foil substrate is challenging, with respect to well-established copper substrate, given that the Al foil has a much lower melting point ($\sim$660 °C) and limited catalytic capability.[25] Therefore, we turned to plasma-enhanced chemical vapor deposition (PECVD) technology, which could help fragment the precursors at relatively lower temperature to accomplish the synthesis of graphene on Al foil at 600 °C (See the Methods section in the Supporting Information for details). Beyond, the community comes to appreciate the significance of the mass production of graphene-based

materials to fully release its potentials.[26−28] Here, a prototypical setup was built to mass produce hierarchical graphene on Al foil. The basics of setup design here is to customize the PECVD technology into roll-to-roll (R2R) configuration that we developed previously (see Figure 2a, as well as Figure S1 in the Supporting Information).[29]

During the synthesis of graphene on Al foil, we observed a clear-cut morphology evolution. At the initial stage, the synthesized graphene was planar and there was no obvious color change of Al foil (see Figure S2 in the Supporting Information).[25] With the elongation of the growth time, the Al foil turned black (Figure 2b) and the vertical branches emerged, as clearly shown in the scanning electron microscopy (SEM) and atomic force microscopy (AFM) images (see Figure 2c, as well as Figure S3a in the Supporting Information). The height of the vertical branch is $\sim$300 nm (see Figure S3b in the Supporting Information). The mass increase of Al foil after hierarchical graphene synthesis is ca. 1%−2%.

To unveil the structural details of as-synthesized hierarchical graphene on Al foil, we performed cross-sectional transmission electron microscopy (TEM) studies. The high-angle annular dark-field scanning transmission electron microscopy (HAADF-STEM) image and elemental mappings unambiguously confirmed that the as-synthesized graphene was composed of a planar basal layer (ca. 20−30 nm) and vertical divergent branches, and the planar basal layer is in tight and conformal contact with aluminum oxide beneath (see Figures 2d and 2e). High-resolution cross-sectional TEM images clearly showed that both the basal layer and vertical branches of as-synthesized graphene were highly graphitized (see Figure 2f). Furthermore, it seems that the emergence of the vertical branch is due to crystal mismatch, as reported previously.[30]
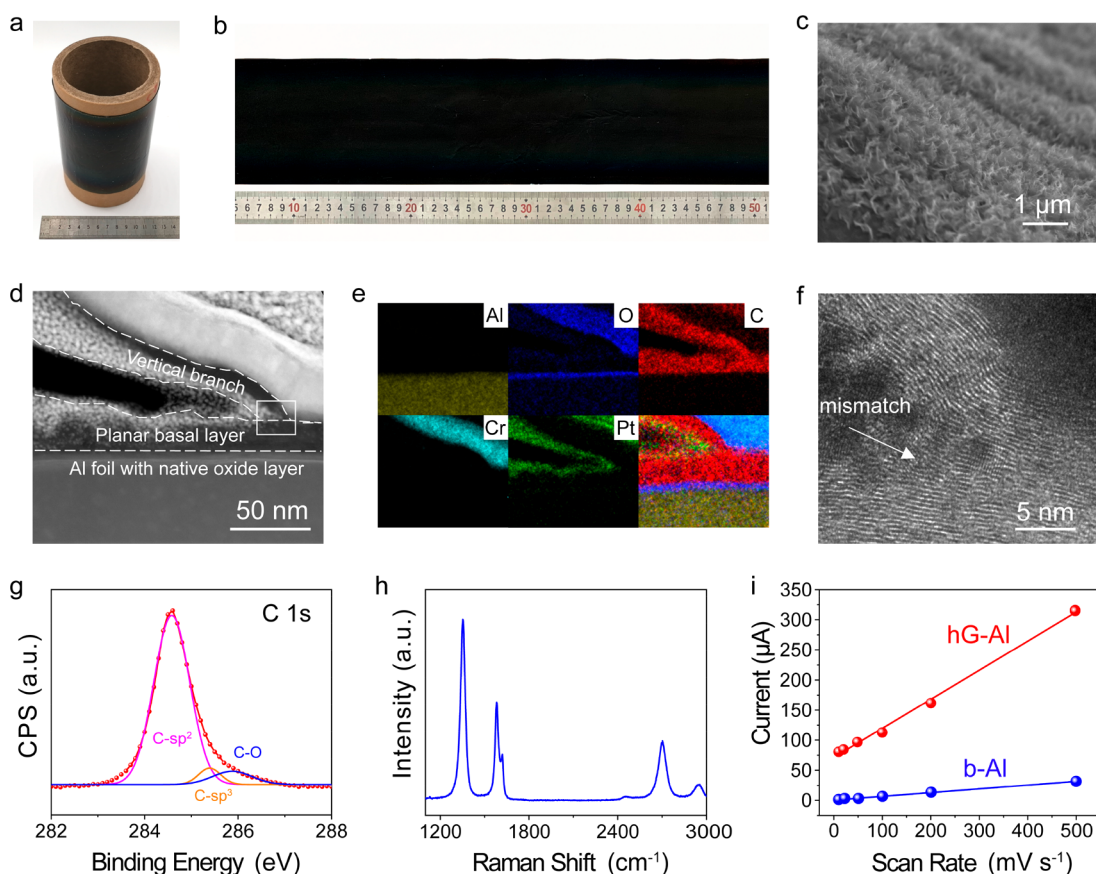
Figure 2. Synthesis and characterization of hierarchical graphene on an Al current collector. (a) Photograph of roll-to-roll (R2R) synthesized hG-Al foil. (b) Photograph of as-synthesized hG-Al foil, whose color was black. (c) Side-view scanning electron microscopy (SEM) image of hG-Al foil from a tilted view. (d) Cross-sectional high-angle annular dark-field scanning transmission electron microscopy (HAADF-STEM) image of hG-Al foil. (e) Elemental mappings corresponding to panel (d). Cr and Pt were thermally evaporated and sputtered sequentially to protect graphene from possible damage during sampling. (f) High-resolution cross-sectional TEM image of the rectangle portion in panel (d). (g, h) X-ray photoemission spectroscopy (XPS) and Raman spectroscopy of as-synthesized hG-Al foil, respectively. (i) Electrochemically active surface area (ECSA) of bare Al foil and as-synthesized hG-Al foil.

X-ray photoemission spectroscopy (XPS) also confirmed that the planar basal layer was chemically bound to aluminum oxide (Figure 2g).[19] Raman spectroscopy of as-synthesized graphene showed a strong D peak (Figure 2h), implying its defective nature (e.g., the observed mismatch).[31] Rationally, these defects can be ascribed to the low synthesis temperature (600 °C), much lower than the synthesis temperature of graphene on other substrates (e.g., ~1000 °C on Cu). Self-evidently, such vertical branches would significantly increase the contact areas between CC and EM. Quantitative electrochemically active surface area (ECSA) measurements (Figure 2i) indicated that the ECSA of hG-Al was 32.2 cm^2 per square centimeter geometrically (cm^2 cm^{-2}), which is ~1 order of magnitude higher than that of bare Al foil (2.5 cm^2 cm^{-2}).

Intuitively, a weak adhesion strength between the CCs and EMs means the easy delamination of EMs from CCs. It could significantly disqualify the electrode yield during the manufacturing process and degrade the electrode for an enduring operation.[32,33] Great significance is thus attached to enhancing the adhesion strength between the current collector and electrode materials. The dramatically structural difference between b-Al and hG-Al foil motivated us to investigate their adhesion strengths.

Commercially available olivine-type lithium iron phosphate (LiFePO$_4$, abbreviated as LFP; see Figure S4 in the Supporting Information) was used as a model system for study. (See the Methods Section in the Supporting Information for details regarding electrode fabrication.) The mechanical peeling-off tests showed that the average adhesion strength of the LFP electrode on b-Al was only ~4.21 N m^{-1}, but was up to 20.50 N m^{-1} on the hG-Al current collector (see Figure 3a). The excellent adhesion property was ascribed to three concatenated factors deriving from the unique configuration of the hG-Al current collector:

(i) the vertical graphene branches dramatically increase the van der Waals interaction areas with electrode, as indicated by the ECSA tests in Figure 2i;

(ii) the strong van der Waals interactions between the vertical graphene branches and planar graphene basal layer due to almost conformal contact; and

(iii) the bindings were supposed to be robust, since there exists strong chemical bonds between the planar graphene and Al foil.

A good adhesion property of hG-Al not only facilitates the electrode manufacturing, but also implies a powerful electronic network between the current collector and electrode materials. Systematic electric measurements are then performed to quantify this effect. In comparison with the b-Al current collector (Figure 3b), the electrode sheet resistance on the hG-Al current collector is reduced by more than 5 orders of
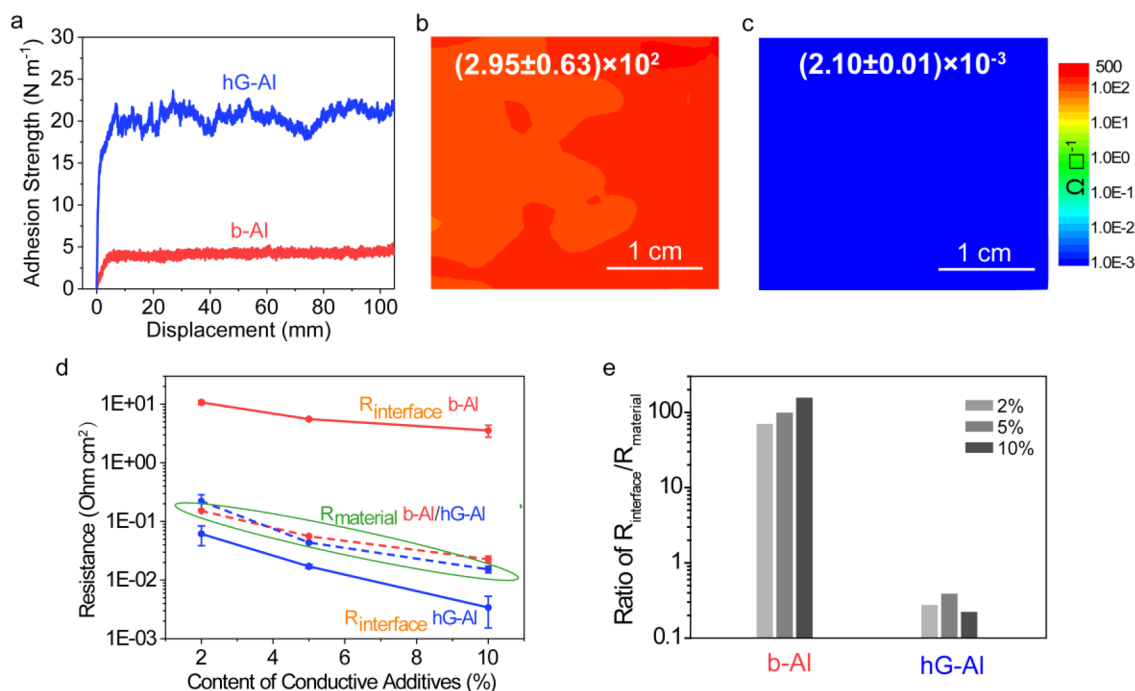
Figure 3. Interfacial properties of a hierarchical graphene engineered Al current collector. (a) The force−displacement curves of the mechanical peeling-off tests of LFP electrodes on different current collectors. (b, c) Electric sheet resistance mappings of LFP electrode on b-Al (panel (b)) and hG-Al (panel (c)). The mass ratio of LFP:conductive additives:PVDF binders is 90:5:5. (d) The material resistance ($R_{material}$) and interfacial resistance ($R_{interface}$) of LFP electrodes with varied content of conductive additives on different current collectors. (e) Ratio of interfacial resistance ($R_{interface}$) and material resistance ($R_{material}$) of LFP electrodes with varied content of conductive additives (i.e., 2%, 5%, 10%) on different CCs.

magnitude (see Figure 3c). Furthermore, the sheet resistance of electrode on b-Al current collector could be hardly reduced by increasing the content of conductive additives, while the sheet resistance of the electrode on the hG-Al current collector was always kept at a minimal level, regardless of the content of conductive additives (see Figure S5 in the Supporting Information). Notably, previous work has shown that a graphene-coated Al current collector could only reduce the electrode sheet resistance by ca. 1 order of magnitude.[23] The underperformance of graphene-coated Al current collector could be attributed to the electrically insulating binder used and rather limited ECSA induced by surface wrinkles.

Given that the electric resistance of the entire electrode is composed of the interfacial resistance ($R_{interface}$) and material resistance ($R_{material}$),[20] we further measured the $R_{interface}$ and $R_{material}$ to probe how the interlayer functions quantitatively. As shown in Figure 3d, the $R_{material}$ values of the electrodes were independent of the CC used and can be efficiently reduced with increased conductive additive content. However, the $R_{interface}$ of the electrode is considerably dependent on the CCs used. Despite the high content of conductive additives used, the $R_{interface}$ of the b-Al current collector is always kept at a high level and is ca. 2 orders of magnitude higher than $R_{material}$. Most strikingly, the $R_{interface}$ value of the hG-Al current collector can be reduced by more than 2 orders of magnitude, to a level lower than $R_{material}$. Moreover, it can be seen that the entire electrode resistance on the b-Al current collector is fairly dominated by their interfacial resistance, whereas the interfacial resistance on the hG-Al current collector is virtually eliminated nonetheless (see Figure 3e). Previous results have reported that the $R_{interface}$ value of a carbon-coated Al current collector is reduced by only ∼1 order of magnitude.[20] Compared with as-synthesized hierarchical graphene interlayer,

the carbon-based interlayer is relatively thick (on the micrometer scale) with insulating binders used, which thus leads to its restrained capability in reducing the interfacial resistance. Reminiscent of the aforementioned underperformance of graphene-coated Al current collector,[23] our systematic measurements unambiguously identify the most profound mesoscopic factor influencing the electrode resistance (i.e., the quality of the CC/EM interface) and quantify its influence.

After the systematic quantitative analyses of the interfacial properties of CCs, we then examined the electrochemical performance of LFP electrodes on different current collectors. Both half-cell and full-cell tests were conducted (See the Methods section in the Supporting Information for details). It has been accepted within the community that, when the mass load of the electrode materials is decent, the electrochemical results are, therefore, more informative to guiding the battery design.[34,35] To this end, the mass load of LFP electrodes used here is relatively thick, which is up to 12 mg per square centimeter and is close to that in commercial LIBs.

First, the electrochemical performances of the LFP electrode on different current collectors were examined in half-cell configuration (Figure 4a). At a low current density of no more than 1 C (1 C = 171 mA g^{-1}), LFP electrodes on different current collectors showed no prominent difference. However, with the increase of current density, the LFP electrode on the b-Al current collector showed a dramatic degradation, while the LFP electrode on the hG-Al current collector still had decent performances. For example, the LFP electrode on the b-Al current collector almost completely failed to function at 4 C, while the average specific discharge capacities of LFP electrodes on hG-Al current collector at 20 C was still up to 43 mAh per gram, respectively. Furthermore, the complete recovery of discharge capacities of both electrodes at low rate,
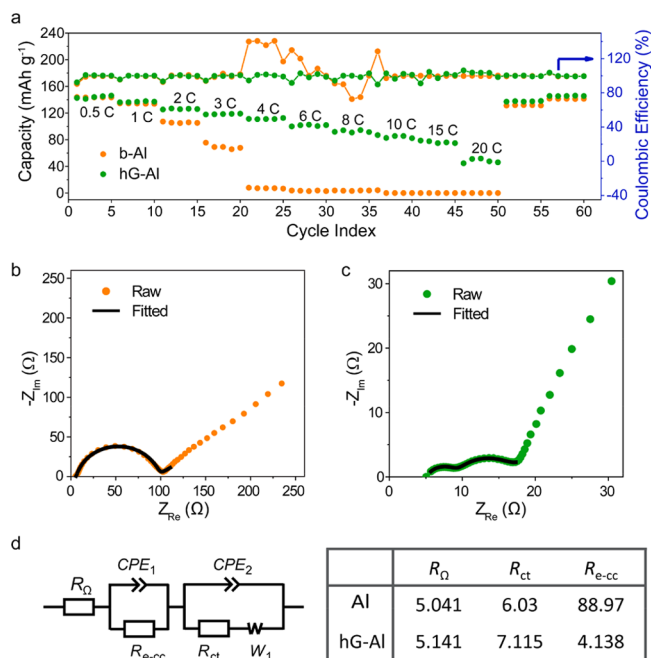
Figure 4. Half-cell electrochemical performance of LFP electrode on different current collectors: (a) rate performance of LFP electrode on bare Al and hG-Al foil current collectors; (b, c) electrochemical impedance spectroscopies of the LFP electrode on bare Al and hG-Al foil current collectors, respectively; and (d) the equivalent circuit used for the analyses of electrochemical impedance spectroscopies and the extrapolated fit results. During the half-cell test, the rate performance was tested with an equal charge and discharge current density.

again following high rate tests, definitely proves that their distinct performances at high rate are intrinsic to the electrode.

Electrochemical impedance spectroscopy (EIS) was widely employed as a noninvasive method to get underlying insights. However, it is rather delicate and even ambiguous to interpret the EIS. For instance, the semicircles in the high-frequency regime in the Nyquist plot of EIS could be interpreted as charge transfer resistance at the electrode/electrolyte interface, the resistance between CC and EM, or electrolyte resistance within the electrode pores, etc.[36,37] Our results showed that the main EIS difference of the LFP electrode in the b-Al current collector and the hG-Al current collector is the semicircles in the high-frequency region (see Figures 4b and 4c). In light of the electric interfacial resistances shown in Figure 3d, it is thus reasonable to infer that the semicircle in the high-frequency region correspond to the resistance between CC and EM. Our results echo those of very recent results, which indicate that the semicircles in the high-frequency regime of EIS should be attributed to the interfacial resistance.[37] An equivalent circuit then was built to simulate the EIS curves (Figure 4d). The intercept of the EIS curve on the real axis represents the ohmic resistance (R_Ω), and the slope lines at low frequency are represented by the Warburg impedance (W_1). In the high-frequency region of semicircles, the electrode/current collector interface impedance is composed of $R_{e\text{-cc}}$ and CPE_1, and the charge transfer impedance is composed of R_{ct} and CPE_2, in which the constant phase elements (CPE_1 and CPE_2) replace the capacitive elements to take into account the geometric factor of the interfaces. The fit results of EIS indicate that LFP electrodes on b-Al and hG-Al have very similar Ohmic resistance (R_Ω) and charge-transfer resistance (R_{ct}) values. However, the resistance between electrodes and current

collectors ($R_{e\text{-cc}}$) are dramatically different. In detail, the $R_{e\text{-cc}}$ value of b-Al is ~20-fold higher than that of hG-Al.

Finally, the electrochemical performances of the LFP electrode on different CSs were further tested in full cell configuration. Artificial graphite (see Figure S6 in the Supporting Information) or lithium titanium oxide ($Li_4Ti_5O_{12}$, abbreviated as LTO; see Figure S7 in the Supporting Information) were paired as anodes.

Even though fast charging looms more and more urgent for rechargeable batteries,[16] it is still a great challenge, particularly for graphite, which is known for being plagued by sluggish kinetics and potential dendrite formation on surface.[38] Therefore, for the full cell tests using the artificial graphite anode, the charge current density was maintained at 0.5 C (1 C = 171 mA g^{-1}), while the discharge rate was sequentially tuned.

It can be seen that the LFP-graphite full cell using the b-Al current collector showed a dramatic polarization increase and fast capacity decay with the increase of discharge current density (see Figure 5a). In comparison, the discharge
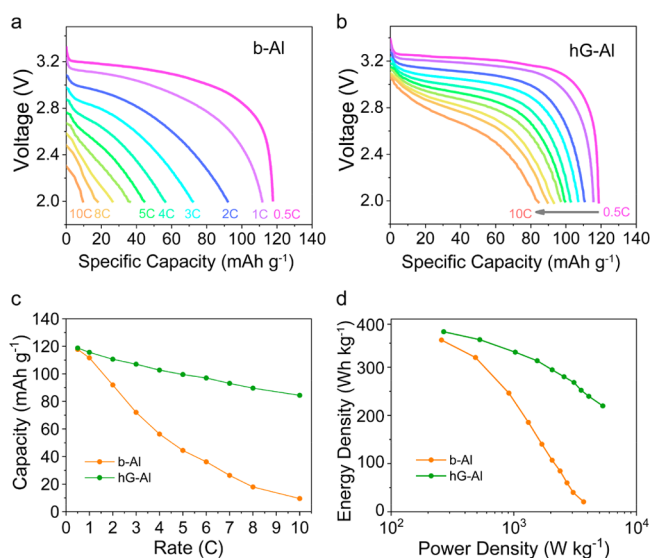
Figure 5. Full-cell electrochemical performance of the LFP electrode on different current collectors paired with an artificial graphite anode: (a, b) the discharge curves of LFP electrode on bare Al and hG-Al foil current collectors in full cell test, respectively; (c) the specific discharge capacity of the LFP electrode on different CC; and (d) the Ragone plot of LFP electrode on different CC.

polarizations of the full cell using hG-Al current collector was significantly inhibited (Figure 5b). Similar to half-cell EIS results, full cell with hG-Al current collector has a much smaller semicircle in the high-frequency region, i.e., smaller resistance between electrodes and current collectors (Figure S8 in the Supporting Information). As a result, the full cell using the hG-Al current collector delivered a much-improved discharge performance, particularly at higher current density (Figure 5c). Finally, the energy density and power density of LFP electrodes on different current collectors were calculated (see Figure 5d and Table S1 in the Supporting Information). The LFP electrode on the hG-Al current collector could deliver a power density output of ~5300 W kg^{-1} at an energy density of ~220 W h kg^{-1}, whereas the LFP electrode on the b-Al current collector could deliver only ~3700 W kg^{-1} at ~21 W h kg^{-1}. Full-cell tests using LTO anodes also corroborated

that the LFP using the hG-Al current collector delivered better electrochemical performance at high current density, much better energy density and power density output, and smaller resistance between electrodes and current collectors in EIS tests (see Figure S9 and Table S2 in the Supporting Information).

We note that the differences of electrochemical performances of electrodes on different CCs were not as dramatic as those of their electric resistance. This noncommensuration is presumably ascribed to the fact that LIBs require the synergy of both the electron and the Li ion.[15]

By growing hierarchical graphene directly on commercial Al CCs, we build up a model system to study the interfacial properties of CCs quantitatively. Our systematic studies highlight the nontrivial role of interfacial properties of the CC at the mesoscopic electrode level. Remarkably, our results show that the interfacial resistance between CC and EM, in truth, dominates the entire electrode resistance. Hierarchical graphene directly grown on the Al current collector, which can serve as a powerful interlayer between the CC and EM, could, in fact, eliminate the awesome interfacial resistance. Electrochemically, it delivers a promoted energy density−power density output accordingly. A similar philosophy could be extended to other electrochemical energy storage devices (e.g., the emerging all solid LIBs,[39] supercapacitors,[24,40] and other monovalent or multivalent batteries[41]). Moreover, for the emerging ultrathick electrode design, whereby the footprints of passive CC can be reduced to enhance the available energy density of the packaged LIB,[35,42] it can be reasoned that eliminating the interfacial resistance between current collector and electrode materials therein would be of more significance. However, great cautions should be taken when graphene or one of its relatives is used to enhance the interfacial properties of the widely utilized anode Cu current collector, considering that graphene might consume lots of Li^+ irreversibly, which means the degradation of the highly valued initial Coulombic efficiency.

Reminiscent of our previous work confirming its enhanced anticorrosion properties at the graphene-engineered Al current collector/electrolyte interface,[25] the graphene skin layer enables commercial Al foil to have almost ideal interfaces with both electrolyte and electrode materials when used as a cathode current collector in LIBs. Moreover, a prototypical mass production method of hierarchical graphene synthesis on metal foil was shown, demonstrating its technical scalability. Honestly, the present bottleneck for its commercialization lies in the low synthesis efficiency and high cost, despite the synthesis being performed at relatively low temperature. Provided the cost-benefit tradeoff could be validated in the future, our work might hopefully foster a niche graphene market.

■ ASSOCIATED CONTENT

Ⓢ Supporting Information

The Supporting Information is available free of charge at https://pubs.acs.org/doi/10.1021/acs.nanolett.0c00348.

Experimental procedure; supplemental figures and tables (PDF)

■ AUTHOR INFORMATION

Corresponding Authors

Hailin Peng − *Center for Nanochemistry, Beijing Science and Engineering Center for Nanocarbons, Beijing National Laboratory for Molecular Sciences, College of Chemistry and Molecular Engineering, Peking University, Beijing 100871, People's Republic of China; Beijing Graphene Institute (BGI), Beijing 100095, People's Republic of China;* ⓘ orcid.org/0000-0003-1569-0238; Email: hlpeng@pku.edu.cn

Zhongfan Liu − *Center for Nanochemistry, Beijing Science and Engineering Center for Nanocarbons, Beijing National Laboratory for Molecular Sciences, College of Chemistry and Molecular Engineering, Peking University, Beijing 100871, People's Republic of China; Beijing Graphene Institute (BGI), Beijing 100095, People's Republic of China;* ⓘ orcid.org/0000-0003-0065-7988; Email: zfliu@pku.edu.cn

Authors

Mingzhan Wang − *Center for Nanochemistry, Beijing Science and Engineering Center for Nanocarbons, Beijing National Laboratory for Molecular Sciences, College of Chemistry and Molecular Engineering, Peking University, Beijing 100871, People's Republic of China;* ⓘ orcid.org/0000-0003-1956-9769

Hao Yang − *Center for Nanochemistry, Beijing Science and Engineering Center for Nanocarbons, Beijing National Laboratory for Molecular Sciences, College of Chemistry and Molecular Engineering and Academy for Advanced Interdisciplinary Studies, Peking University, Beijing 100871, People's Republic of China*

Kexin Wang − *Center for Nanochemistry, Beijing Science and Engineering Center for Nanocarbons, Beijing National Laboratory for Molecular Sciences, College of Chemistry and Molecular Engineering, Peking University, Beijing 100871, People's Republic of China*

Shulin Chen − *Center for Nanochemistry, Beijing Science and Engineering Center for Nanocarbons, Beijing National Laboratory for Molecular Sciences, College of Chemistry and Molecular Engineering and Electron Microscopy Laboratory, and International Centre for Quantum Materials, School of Physics, Peking University, Beijing 100871, People's Republic of China; State Key Laboratory of Advanced Welding and Joining, Harbin Institute of Technology, Harbin 150001, People's Republic of China*

Haina Ci − *Center for Nanochemistry, Beijing Science and Engineering Center for Nanocarbons, Beijing National Laboratory for Molecular Sciences, College of Chemistry and Molecular Engineering and Academy for Advanced Interdisciplinary Studies, Peking University, Beijing 100871, People's Republic of China*

Liurong Shi − *Center for Nanochemistry, Beijing Science and Engineering Center for Nanocarbons, Beijing National Laboratory for Molecular Sciences, College of Chemistry and Molecular Engineering, Peking University, Beijing 100871, People's Republic of China*

Jingyuan Shan − *Center for Nanochemistry, Beijing Science and Engineering Center for Nanocarbons, Beijing National Laboratory for Molecular Sciences, College of Chemistry and Molecular Engineering and Academy for Advanced Interdisciplinary Studies, Peking University, Beijing 100871, People's Republic of China*

Shipu Xu − *Center for Nanochemistry, Beijing Science and Engineering Center for Nanocarbons, Beijing National*

Laboratory for Molecular Sciences, College of Chemistry and Molecular Engineering, Peking University, Beijing 100871, People's Republic of China

Qinci Wu − Center for Nanochemistry, Beijing Science and Engineering Center for Nanocarbons, Beijing National Laboratory for Molecular Sciences, College of Chemistry and Molecular Engineering, Peking University, Beijing 100871, People's Republic of China

Chongzhen Wang − Center for Nanochemistry, Beijing Science and Engineering Center for Nanocarbons, Beijing National Laboratory for Molecular Sciences, College of Chemistry and Molecular Engineering, Peking University, Beijing 100871, People's Republic of China

Miao Tang − Center for Nanochemistry, Beijing Science and Engineering Center for Nanocarbons, Beijing National Laboratory for Molecular Sciences, College of Chemistry and Molecular Engineering, Peking University, Beijing 100871, People's Republic of China

Peng Gao − Electron Microscopy Laboratory, and International Centre for Quantum Materials, School of Physics, Peking University, Beijing 100871, People's Republic of China; Collaborative Innovation Centre for Quantum Matter, Beijing 100871, China; orcid.org/0000-0003-0860-5525

Complete contact information is available at:
https://pubs.acs.org/10.1021/acs.nanolett.0c00348

Author Contributions

[▽]These authors contributed equally

Author Contributions

M.W., Z.L., and H.P. conceived the idea. M.W., H.Y., and K.W. synthesized the hierarchical graphene on Al foil with the assistance of H.C. and M. T. M.W. and H.Y. designed the electrodes and conducted the electrical and electrochemical measurements. S.C. and P.G. conducted TEM characterization. Z.L. and H.P. supervised the project. M.W. and H.P. wrote the manuscript. All authors discussed the results and commented on the manuscript.

Notes

The authors declare no competing financial interest.

■ REFERENCES

(1) Goodenough, J. B.; Park, K.-S. The Li-Ion Rechargeable Battery: A Perspective. *J. Am. Chem. Soc.* **2013**, *135*, 1167.

(2) Armand, M.; Tarascon, J. M. Building better batteries. *Nature* **2008**, *451*, 652.

(3) Bruce, P. G.; Scrosati, B.; Tarascon, J.-M. Nanomaterials for rechargeable lithium batteries. *Angew. Chem., Int. Ed.* **2008**, *47*, 2930.

(4) Bruce, P. G.; Freunberger, S. A.; Hardwick, L. J.; Tarascon, J.-M. Li-O$_2$ and Li-S batteries with high energy storage. *Nat. Mater.* **2012**, *11*, 19.

(5) Goodenough, J. B. Cathode materials: A personal perspective. *J. Power Sources* **2007**, *174*, 996.

(6) Liu, N.; Lu, Z.; Zhao, J.; McDowell, M. T.; Lee, H.-W.; Zhao, W.; Cui, Y. A pomegranate-inspired nanoscale design for large-volume-change lithium battery anodes. *Nat. Nanotechnol.* **2014**, *9*, 187.

(7) Xu, K. Electrolytes and Interphases in Li-Ion Batteries and Beyond. *Chem. Rev.* **2014**, *114*, 11503.

(8) Tan, S.; Ji, Y. J.; Zhang, Z. R.; Yang, Y. Recent Progress in Research on High-Voltage Electrolytes for Lithium-Ion Batteries. *ChemPhysChem* **2014**, *15*, 1956.

(9) Wood, D. L., III; Li, J.; Daniel, C. Prospects for reducing the processing cost of lithium ion batteries. *J. Power Sources* **2015**, *275*, 234.

(10) Li, J.; Daniel, C.; Wood, D. Materials processing for lithium-ion batteries. *J. Power Sources* **2011**, *196*, 2452.

(11) Myung, S.-T.; Hitoshi, Y.; Sun, Y.-K. Electrochemical behavior and passivation of current collectors in lithium-ion batteries. *J. Mater. Chem.* **2011**, *21*, 9891.

(12) Arico, A. S.; Bruce, P.; Scrosati, B.; Tarascon, J. M.; Van Schalkwijk, W. Nanostructured materials for advanced energy conversion and storage devices. *Nat. Mater.* **2005**, *4*, 366.

(13) Sun, C.; Rajasekhara, S.; Goodenough, J. B.; Zhou, F. Monodisperse Porous LiFePO$_4$ Microspheres for a High Power Li-Ion Battery Cathode. *J. Am. Chem. Soc.* **2011**, *133*, 2132.

(14) Arai, Y.; Kunisawa, M.; Yamaguchi, T.; Yokouchi, H.; Matsuo, A.; Ohmori, M. Studies of SDXTM on the Boundary Resistance between Aluminum Current Collectors and Cathode Active Material Layers. *ECS Trans.* **2013**, *50*, 153.

(15) Pan, H. L.; Hu, Y. S.; Li, H.; Chen, L. Q. Significant effect of electron transfer between current collector and active material on high rate performance of Li$_4$Ti$_5$O$_{12}$. *Chin. Phys. B* **2011**, *20*, 118202.

(16) Liu, Y. Y.; Zhu, Y. Y.; Cui, Y. Challenges and opportunities towards fast-charging battery materials. *Nat. Energy* **2019**, *4*, 540.

(17) Nakanishi, S.; Suzuki, T.; Cui, Q.; Akikusa, J.; Nakamura, K. Effect of surface treatment for aluminum foils on discharge properties of lithium-ion battery. *Trans. Nonferrous Met. Soc. China* **2014**, *24*, 2314.

(18) Portet, C.; Taberna, P. L.; Simon, P.; Laberty-Robert, C. Modification of Al current collector surface by sol-gel deposit for carbon-carbon supercapacitor applications. *Electrochim. Acta* **2004**, *49*, 905.

(19) Striebel, K.; Shim, J.; Sierra, A.; Yang, H.; Song, X. Y.; Kostecki, R.; McCarthy, K. The development of low cost LiFePO$_4$-based high power lithium-ion batteries. *J. Power Sources* **2005**, *146*, 33.

(20) Takeda, A.; Nakamura, T.; Yokouchi, H.; Tomozawa, H. The mechanism of decreasing resistance by SDX (TM) in lithium ion battery. *ECS Trans.* **2017**, *75*, 17.

(21) Rytel, K.; Waszak, D.; Kedzierski, K.; Wrobel, D. Novel method of current collector coating by multiwalled carbon nanotube Langmuir layer for enhanced power performance of LiMn$_2$O$_4$ electrode of Li-ion batteries. *Electrochim. Acta* **2016**, *222*, 921.

(22) Jiang, J.; Nie, P.; Ding, B.; Wu, W.; Chang, Z.; Wu, Y.; Dou, H.; Zhang, X. Effect of Graphene Modified Cu Current Collector on the Performance of Li$_4$Ti$_5$O$_{12}$ Anode for Lithium-Ion Batteries. *ACS Appl. Mater. Interfaces* **2016**, *8*, 30926.

(23) Wen, L.; Liang, J.; Liu, C. M.; Chen, J.; Huang, Q. G.; Luo, H. Z.; Li, F. Li$_4$Ti$_5$O$_{12}$ on Graphene for High Rate Lithium Ion Batteries. *J. Electrochem. Soc.* **2016**, *163*, A2951.

(24) Bo, Z.; Zhu, W. G.; Ma, W.; Wen, Z. H.; Shuai, X. R.; Chen, J. H.; Yan, J. H.; Wang, Z. H.; Cen, K. F.; Feng, X. L. Vertically Oriented Graphene Bridging Active-Layer/Current-Collector Interface for Ultrahigh Rate Supercapacitors. *Adv. Mater.* **2013**, *25*, 5799.

(25) Wang, M. Z.; Tang, M.; Chen, S. L.; Ci, H. N.; Wang, K. X.; Shi, L. R.; Lin, L.; Ren, H. Y.; Shan, J. Y.; Gao, P.; Liu, Z. F.; Peng, H. L. Graphene-Armored Aluminum Foil with Enhanced Anticorrosion

Performance as Current Collectors for Lithium-Ion Battery. *Adv. Mater.* **2017**, *29*, 1703882.

(26) Ren, W. C.; Cheng, H. M. The global growth of graphene. *Nat. Nanotechnol.* **2014**, *9*, 726.

(27) Bae, S.; Kim, H.; Lee, Y.; Xu, X.; Park, J.-S.; Zheng, Y.; Balakrishnan, J.; Lei, T.; Kim, H. R.; Song, Y. I.; Kim, Y.-J.; Kim, K. S.; Ozyilmaz, B.; Ahn, J.-H.; Hong, B. H.; Iijima, S. Roll-to-roll production of 30-in. graphene films for transparent electrodes. *Nat. Nanotechnol.* **2010**, *5*, 574.

(28) Lin, L.; Peng, H. L.; Liu, Z. F. Synthesis challenges for graphene industry. *Nat. Mater.* **2019**, *18*, 520.

(29) Deng, B.; Hsu, P. C.; Chen, G. C.; Chandrashekar, B. N.; Liao, L.; Ayitimuda, Z.; Wu, J. X.; Guo, Y. F.; Lin, L.; Zhou, Y.; Aisijiang, M.; Xie, Q.; Cui, Y.; Liu, Z. F.; Peng, H. L. Roll-to-Roll Encapsulation of Metal Nanowires between Graphene and Plastic Substrate for High-Performance Flexible Transparent Electrodes. *Nano Lett.* **2015**, *15*, 4206.

(30) Zhao, J.; Shaygan, M.; Eckert, J.; Meyyappan, M.; Ruemmeli, M. H. A Growth Mechanism for Free-Standing Vertical Graphene. *Nano Lett.* **2014**, *14*, 3064.

(31) Ferrari, A. C. Raman spectroscopy of graphene and graphite: Disorder, electron-phonon coupling, doping and nonadiabatic effects. *Solid State Commun.* **2007**, *143*, 47.

(32) Versaci, D.; Nasi, R.; Zubair, U.; Amici, J.; Sgroi, M.; Dumitrescu, M. A.; Francia, C.; Bodoardo, S.; Penazzi, N. New eco-friendly low-cost binders for Li-ion anodes. *J. Solid State Electrochem.* **2017**, *21*, 3429.

(33) Kovalenko, I.; Zdyrko, B.; Magasinski, A.; Hertzberg, B.; Milicev, Z.; Burtovyy, R.; Luzinov, I.; Yushin, G. A Major Constituent of Brown Algae for Use in High-Capacity Li-Ion Batteries. *Science* **2011**, *334*, 75.

(34) Gogotsi, Y.; Simon, P. True Performance Metrics in Electrochemical Energy Storage. *Science* **2011**, *334*, 917.

(35) Sun, H. T.; Zhu, J.; Baumann, D.; Peng, L. L.; Xu, Y. X.; Shakir, I.; Huang, Y.; Duan, X. F. Hierarchical 3D electrodes for electrochemical energy storage. *Nat. Rev. Mater.* **2019**, *4*, 45.

(36) Mei, B. A.; Munteshari, O.; Lau, J.; Dunn, B.; Pilon, L. Physical Interpretations of Nyquist Plots for EDLC Electrodes and Devices. *J. Phys. Chem. C* **2018**, *122*, 194.

(37) Allison, A.; Andreas, H. A. Minimizing the Nyquist-plot semi-circle of pseudocapacitive manganese oxides through modification of the oxide-substrate interface resistance. *J. Power Sources* **2019**, *426*, 93.

(38) Zaghib, K.; Goodenough, J. B.; Mauger, A.; Julien, C. Unsupported claims of ultrafast charging of LiFePO4 Li-ion batteries. *J. Power Sources* **2009**, *194*, 1021.

(39) Kato, Y.; Hori, S.; Saito, T.; Suzuki, K.; Hirayama, M.; Mitsui, A.; Yonemura, M.; Iba, H.; Kanno, R. High-power all-solid-state batteries using sulfide superionic conductors. *Nat. Energy* **2016**, *1*, 16030.

(40) Wu, H. C.; Lin, Y. P.; Lee, E.; Lin, W. T.; Hu, J. K.; Chen, H. C.; Wu, N. L. High-performance carbon-based supercapacitors using Al current-collector with conformal carbon coating. *Mater. Chem. Phys.* **2009**, *117*, 294.

(41) Muldoon, J.; Bucur, C. B.; Gregory, T. Quest for Nonaqueous Multivalent Secondary Batteries: Magnesium and Beyond. *Chem. Rev.* **2014**, *114*, 11683.

(42) Li, Y. J.; Fu, K.; Chen, C. J.; Luo, W.; Gao, T. T.; Xu, S. M.; Dai, J. Q.; Pastel, G.; Wang, Y. B.; Liu, B. Y.; Song, J. W.; Chen, Y. N.; Yang, C. P.; Hu, L. B. Enabling High-Areal-Capacity Lithium-Sulfur Batteries: Designing Anisotropic and Low-Tortuosity Porous Architectures. *ACS Nano* **2017**, *11*, 4801.